Non-linear effects on the resonant frequencies of a cantilevered plate

Rocío F. Arellano Castro[1], Lancelot Guillamot[2], Anne Cros[1], Christophe Eloy[3]

[1] *Departamento de Física, Universidad de Guadalajara, Mexico*
[2] *Aix-Marseille Université, IUT GTE, Marseille, France*
[3] *Aix-Marseille Université, IRPHE UMR 7342, CNRS, Marseille, France*

Abstract

In this paper, we address experimentally and theoretically the non-linear effects on the resonance of a periodically-forced cantilevered plate immersed in a fluid at rest. Experiments are performed with small aspect-ratio plates made of two different materials. When forced harmonically at their leading edges, these plates exhibit resonances for their first 3 structural modes. The frequencies at these resonances decrease when the forcing amplitude is increased, revealing the presence of non-linear effects. To model this phenomenon, a theoretical model is developed, which takes into account both resistive and reactive forces exerted by the fluid on the plate. By carrying out a weakly non-linear analysis, the frequencies at the resonances can then be determined. Model and experiments are in good agreement, showing that a weakly non-linear approach is suited to this kind of fluid-structure interaction and could be applied, in the future, to engineering problems such as energy harvesting with a fluttering plate or the biological problem of aquatic propulsion with a flexible fin.

Keywords: resonant frequencies, non-linear effects, cantilever beam

1. Introduction

One of the most simple example of fluid-structure interaction is the vibration of a cantilever plate in a fluid at rest. Yet, even in this simple example, complex effects may arise and hinder the development of accurate modeling. First, it should be realized that this fluid-structure interaction is strong in the sense that both the plate motion modifies the fluid flow around it and the flow modifies the forces on the plate and thus its dynamics. Second, as soon as the beam deflection is of the order of its length, non-linear effects come into play. These non-linear effects are mainly caused by geometrical effects (as the boundary conditions need to be evaluated on a displaced beam), but may also be caused by non-linearities of the structural constitutive relation (e.g. plastic deformation) or the fluid (e.g. if vorticity is detached). The objective of this paper is to study in an idealized system the effect of weakly non-linear effects on the resonance of a cantilever plate.

Every structure has resonant frequencies associated to its elastic and geometric characteristics. In some cases, the resonant modes are excited on purpose, as for the two-stroke engine (Tenney, 1972; Blair, 1996), the string and wind instruments (Fletcher and Rossing, 1998), radio antennas (Huang and Boyle, 2008), magnetic resonance imaging (Kuperman, 2000) and atomic force microscopes (Sader, 1998; Blom et al., 1992; Ghatkesar et al., 2008). These resonances may also be used to determine the Young's modulus of a sample as it is done in a classical undergraduate experiment (Wilson and Lord Jr., 1973; Turvey, 1990). In other cases, resonance is undesirable and may cause severe damages in architectural constructions, rail transport, aeronautics, or in the automobile industry. In this case, the excitation may be due to instabilities of the fluid-structure interactions such as flutter, galloping, or vortex-induced vibration (Dowell and Hall, 2001; Païdoussis, 1998, 2004).

When a plate vibrates, the forces that the fluid exerts on it can be decomposed into two components: reactive forces and resistive forces. Reactive forces have an inviscid origin and have been modeled in the context of fish swimming by Lighthill (1960, 1971) and recently revived by Candelier et al. (2011, 2013). Their origin is as follows: when a body immersed in a fluid moves, a certain added-mass of fluid is also displaced; the acceleration of this added-mass implies that the body has exerted a certain force on the fluid and that, reactively, the fluid has exerted the opposite force on the body. In the linear regime, or equivalently for small-amplitude deformations, added-mass effects tend to decrease the

resonance frequencies of a structure compared to vibrations *in vacuo*, as they are equivalent to increasing the mass of the structure (the resonant frequencies being inversely proportional to the square root of the structure mass).

Resistive forces are due to viscous effects and, in particular, are present when boundary layers separate and vorticity is detached. They result in drag forces that are, in the limit of large Reynolds numbers, proportional to the square of the normal velocity (Taylor, 1952). Resistive forces, because of this quadratic dependence, are inherently non-linear. They can be taken into account in a weakly non-linear model if some approximations are made (e.g. Lopes et al., 2002). It is usually assumed that resistive and reactive force can be considered separately and that the total force exerted by the fluid is a linear superimposition of the two. Although this assumption could be disputed, we will proceed similarly in the present analysis.

In this work, we will considered both reactive and resistive forces acting on a vibrating plate. Our goal is to assess the importance of the first non-linear effects on the resonant frequencies. The theoretical model will first be introduced in section 2. Then, the setup and the experimental results will be presented in section 3. Finally, a comparison between the two will be drawn in section 4 before proposing a conclusion.

2. Model

2.1. Equation of motion

Consider a flexible rectangular plate of length L and width H clamped at one edge and free at the other (Fig. 1). When the clamped edge is set in motion in the y-direction with angular frequency ω, the deformation of the plate is one-dimensional, i.e. independent of the z-direction. In this case, its deflection can be described by the position vector $\mathbf{x}(s,t) = (x,y)$, which is a function of time and the curvilinear coordinate s measuring the distance from the clamped edge. This plate obeys the Euler-Bernoulli beam equation

$$m\partial_t^2\mathbf{x} + D\partial_s^4\mathbf{x} - \partial_s(\langle T\rangle\partial_s\mathbf{x}) + \langle p\rangle\hat{\mathbf{n}} = 0, \tag{1}$$

with m the plate mass per unit area, D the plate bending rigidity, and T the generalized tension in the plate, which originates from the inextensibility condition. The last term in eqn. (1) comes from pressure forces because of a pressure jump $p(s,z,t)$ across the plate due to the surrounding flow. Finally, the $\hat{\mathbf{n}}$ denotes the unit vector normal to the plate and the brackets denote averaging in the z-direction along the plate width (Eloy et al., 2012). The equation of motion (1) is supplemented by the clamped–free boundary conditions: $y = \partial_s y = 0$ in $s = 0$, and $\partial_s^2 y = \partial_s^3 y = T = 0$ in $s = L$.

In the elongated body limit (i.e. $H \ll L$), pressure forces on the plate can be decomposed into two parts

$$\langle p\rangle = p_{\text{reac.}} + p_{\text{resis.}}, \tag{2}$$

with $p_{\text{reac.}}$ the reactive force and $p_{\text{resis.}}$ the resistive force. The reactive force is physically due to the necessity for the plate to accelerate a certain added mass of fluid when it is set in motion. To accelerate this mass of fluid, a force has to be exerted on it, and reactively the opposite force is exerted on the plate (Lighthill, 1971). The resistive force is simply the drag on the plate due to the crossflow component of the relative velocity between the plate and the fluid. These forces can be written as

$$p_{\text{reac.}} = M\left(\dot{w} - (uw)' + \tfrac{1}{2}w^2\kappa\right), \tag{3}$$

$$p_{\text{resis.}} = \tfrac{1}{2}\rho C_d|w|w, \tag{4}$$

where κ is the plate curvature, $M = \pi\rho H/4$ is the added mass of air per unit area,, C_d is a drag coefficient taken to be $C_d = 1.8$ for a plate (Buchak et al., 2010), dots and primes denote differentiation with respect to t and s respectively, u and w are the longitudinal and normal components of the plate velocity such that $\dot{\mathbf{x}} = u\hat{\mathbf{t}} + w\hat{\mathbf{n}}$ and

$$u = \dot{x}x' + \dot{y}y', \quad w = -\dot{x}y' + \dot{y}x'. \tag{5}$$

The system can be made dimensionless by using L and $L^2\sqrt{m/D}$ as characteristic length and time respectively. The dimensionless variables, noted with asterisks, then becomes:

$$y^* = y/L, \quad x^* = x/L, \quad \omega^* = \omega L^2\sqrt{D/m}. \tag{6}$$

The dimensionless parameters describing the problem are the mass ratio M^*, and the resistive to inertial forces ratio N^* given respectively by

$$M^* = \frac{M}{m} = \frac{\pi\rho H}{4m}, \quad N^* = \frac{\rho C_D L}{m}. \tag{7}$$

These two numbers give the relative scaling of reactive and resistive forces to inertial effects. Hereinafter, except for the dimensionless parameters M^* and N^*, the asterisks will be dropped and, unless stated otherwise, all variables will be assumed dimensionless.

At this point, equation (1), complemented with equations (3–5), describes the non-linear fully-coupled fluid-structure interaction. We will now consider the weakly non-linear regime in order to analyze the response to an harmonic forcing and derive the amplitude equations.

2.2. Weakly non-linear analysis

The weakly non-linear dynamical equation can be found by following a method similar to the one of Yadykin et al. (2001), except that we will also consider non-linearities originating from the fluid forces. First, equations (3–5) are inserted into (1) and the equation is projected onto $\hat{\mathbf{x}}$ and $\hat{\mathbf{y}}$. This yields two coupled differential equations for $x(s,t)$ and $y(s,t)$ respectively. Then, these equations are decoupled by successively eliminating the tension $\langle T\rangle$ using the x-projection and eliminating $x(s,t)$ and its derivatives by using the inextensibility condition. Finally the terms of order larger than $O(y^3)$ are discarded. This method gives a weakly non-linear dynamical equation for $y(s,t)$ of the form

$$\mathcal{L}(y) + f_m(y) + f_D(y) + M^* f_{\text{reac.}}(y) + N^* f_{\text{resis.}}(y) = 0, \tag{8}$$

where $\mathcal{L}$ is the following linear differential operator on y

$$\mathcal{L}(y) = (1 + M^*)\ddot{y} + y'''', \tag{9}$$

$f_{\text{resis.}}$ is a $O(y^2)$ term due to the resistive force

$$f_{\text{resis.}}(y) = \frac{1}{2}|\dot{y}|\dot{y}. \tag{10}$$

and the other terms are non-linear $O(y^3)$ terms given by

$$f_m(y) = y' \int_0^s \left(\dot{y}'^2 + y'\ddot{y}'\right) \mathrm{d}s - y'' \int_s^L \int_0^s \left(\dot{y}'^2 + y'\ddot{y}'\right) \mathrm{d}s\mathrm{d}s, \tag{11}$$

$$f_D(y) = y''''y'^2 + 4\,y'y''y''' + y''^3, \tag{12}$$

$$f_{\text{reac.}}(y) = -3\dot{y}y'\dot{y}' - \frac{1}{2}\dot{y}^2y'' + 2\dot{y}' \int_0^s \dot{y}'y' \mathrm{d}s - y'' \int_s^L y'\ddot{y}\mathrm{d}s. \tag{13}$$

The solution of the linear problem $\mathcal{L}(y_0 \mathrm{e}^{\mathrm{i}\omega t}) = 0$ with clamped-free boundary conditions is

$$y_0(x) = A\left[\cos kx - \cosh kx + \gamma(k)(\sin kx - \sinh kx)\right], \tag{14}$$

with

$$\gamma(k) = \frac{\sin k - \sinh k}{\cos k + \cosh k}, \tag{15}$$

and k solution of

$$\cos k \cosh k + 1 = 0, \tag{16}$$

such that $k \approx 1.875$, 4.694, and 7.855 for the first three eigenmodes and A is the mode amplitude which will be determined by solving the system at the next order. The corresponding (dimensionless) angular eigenfrequencies are given by

$$(1 + M^*)\omega^2 = k^4. \tag{17}$$

To determine the amplitude A of the linear mode, the deflection y is now assumed to be of the form

$$y(s,t) = (Ay_0(s) + y_1(s))\mathrm{e}^{\mathrm{i}\omega t} + \text{c.c.} + \text{h.o.t.}, \tag{18}$$

where y_1 gathers all the terms of order greater than A, c.c. stands for "complex conjugate", and h.o.t. stands for "higher order terms" (which include here higher harmonics). The decomposition (18) is inserted into (8) and the whole equation is multiplied by $y_0 e^{-i\omega t}$, which is the solution of the adjoint linear problem (the problem being self-adjoint). The result is then integrated between 0 and L in order to eliminate the term $\mathcal{L}(y_1 e^{i\omega t})$ and it yields an amplitude equation for A, assuming A is real and positive without loss of generality:

$$-(1 + M^*)\omega^2 + k^4 + i\,\omega^2 N^* dA + \left(l_1 + l_2\omega^2 + l_3 M^*\omega^2\right)A^2 = 0, \tag{19}$$

where the coefficients d and l_i are integrals implying the linear mode y_0 and its derivatives and are given in Table 1 for the first three modes. In this amplitude equation, the first term corresponds to the linear inertial term (including added mass effects), the second term is linked to the linear elastic restoring force, the third term is the non-linear term arising from the resistive force and the last term gather all non-linear effects due to inertial, elastic, and reactive forces. Note that the third term is complex, indicating a damping effect of the resistive forces, as expected.

Table 1: Value of the coefficients appearing in the amplitude equation (19) for the first three modes

mode	k^4	d	l_1	l_2	l_3
1	12.36	2.956	121.3	−9.194	−13.17
2	485.5	2.589	40254	−289.5	−70.14
3	3807	2.528	793096	−2000	−151.3

Once the coefficients appearing in (19) are calculated (see Table 1), the dependence of the eigenfrequencies on the amplitude can be found. For small amplitudes, we recover the linear solution: $\omega = k^2/\sqrt{1 + M^*}$. For larger amplitudes A, the resonant frequencies of the first 3 modes can be found by solving the second order equation (19) for ω and extracting its real part. This calculation leads to frequencies that decrease as A increases (see Fig. 4 below). In this system, non-linearities thus tend to reduce the eigenfrequencies.

3. Experiments

The principle of the experimental setup is illustrated in Fig. 1. The plate is clamped along its height to a rigid axis. This axis is set in vibration in the transversal (y-)direction with a frequency f and a controlled small amplitude. Typically, in the experiments described in this study, f is varied from 0 to 50 Hz and the oscillation amplitude from 0 to 6 mm. A motion sensor allows us to measure the time evolution of the transversal displacement $y(x_0, t)$ at a certain longitudinal coordinate x_0 of the plate. This motion sensor is a CCD laser displacement sensor made by Keyence. Its y-precision is better than 0.2 mm, and time-precision is about 1 ms.

Figure 2 shows the different positions x_0 of the motion sensor depending on the mode studied. The points x_0 are chosen such that they correspond roughly to an anti-node of the eigenmode. The amplitudes A_0 measured at these points can be related to the amplitudes A used in the previous section using equation (14). This correction factor has to be taken into account to compare the experimental measurements with the model.

	plastic plate	aluminium plate
D $(N.m^2)$	3.04×10^{-4}	1.13×10^{-1}
m (kg/m^2)	0.242	0.641
L (cm)	13.4	35.2
H (cm)	5.0	13.1
M^*	0.209	0.209
N^*	1.28	1.28

Table 2: Elastic and geometric characteristics of the plates.

In the present study, we used two different materials for the plate: an aluminum plate and a plastic polyester plate (in practice, we used a x-ray plate). Table 2 shows the elastic and the geometric characteristics of these plates. The dimensions H and L have been chosen so that the dimensionless numbers M^* and N^* are equal for both plates.

The protocol used in the present experiments is the following. The frequency and the amplitude of the harmonic forcing are set to their minimal values. With the motion sensor, the time evolution $y(x_0, t)$ at the point x_0 is measured and the oscillation amplitude A_0 is extracted thus allowing us to determine A. The frequency is then increased by small increments on a large interval (Table 3) to obtain a response curve $A(f)$ for a given forcing amplitude. This process is performed again for higher values of the forcing amplitude.

	plastic plate		aluminium plate	
modes	frequency interval (Hz)	frequency increment (Hz)	frequency interval (Hz)	frequency increment(Hz)
1	[2; 4]	0.2	[1; 2]	0.05
2	[14; 20]	0.2	[7; 10]	0.2
3	[41; 50.5]	0.5	[20; 28]	0.2

Table 3: Frequencies intervals and frequency increments for the plastic plate and the aluminium plate.

An example of a series of resonant curves is shown in Fig. 3. Each of this curve correspond to a frequency response $A(f)$ for a different forcing amplitude. It can be seen that, as the amplitudes of the forcing and of the response increase, the response changes both qualitatively and quantitatively: the peak frequency is shifted toward lower values and the shape of the peak becomes more asymmetric. These two phenomena indicate non-linear effects.

From each of these curves, the coordinates of the maximum have been extracted, and the same has been done for the first three resonances of the two plates. In Fig. 4, the locations of these maxima, made dimensionless using Eqs. (6), have been plotted and compared to the theoretical prediction of the model detailed in section 2. First, it should be noted that the dimensionless frequencies for the two different materials coincide, showing that the material does not play an important role, and thus likely remains in the linearly elastic regime of thin plates (which does not mean that non-linear geometric or fluid effects can be discarded, of course). Second, in both the model and the experiments, aside from minor experimental uncertainties, the resonant frequencies are monotonically decreasing functions of the amplitude. While, for the first mode, this effect is not pronounced as the frequency is roughly constant in the interval accessible ($0 < A/L < 0.013$), for the second mode, the resonant frequencies exhibit a clearer decrease when the forcing amplitude is increased, both in experiments and in the model. The largest variations, however, are observed for the third mode: in this case, frequencies superimpose fairly well, showing that the weakly non-linear effects considered in the model give an accurate description of the frequency shift due to large amplitude deformations.

4. Discussion

In summary, we have addressed theoretically and experimentally how non-linear effects modify the resonant frequencies of a flexible plate forced into harmonic motion. The theoretical model developed here takes into account a resistive force due to the drag experienced by the plate when it oscillates, and it also takes into account a reactive force, which is due to the acceleration of an added-mass of fluid attached to the plate. In addition, a series of experiment has been performed with two different materials, aluminum and a plastic plates. It allowed us to determine the evolution of the resonant frequencies of the first 3 resonant modes as the the forcing amplitude was varied. The experimental data are in good agreement with the model, both showing that the resonant frequency decreases as the forcing amplitude incrases.

This result may have applications to biological and engineering problems. In the biological context, the aquatic propulsion of most animals is based on flexible fins whose amplitude is generally in the non-linear regime. In addition to the present idealized system however, a uniform flow due to the swimming speed has to be considered. This problem has been addressed numerically by Katz and Weihs (1978), Alben (2008), and Michelin and Llewellyn Smith (2009), and experimentally by Heathcote and Gursul (2007) and Marais et al. (2012), among others. Yet, non-linear effects are generally not considered in the analytical models and the approach proposed here could thus be used to gain a

better insight into the importance and implications of non-linear mechanisms in this problem. Another example of a possible application of the present model is to be found in the engineering context. Different methods have indeed been proposed to harvest energy from the flutter of a flexible plate or cylinder (e.g. Peng and Zhu, 2009; Singh et al., 2012; Michelin and Doaré, 2013). Again, concrete applications will likely be for fairly large deformation amplitude whereas most models used so far are linear. The method proposed here could therefore help to understand how non-linearities may affect the performance of energy harvesting and if the devices should be tuned to an optimal flutter amplitude.

Acknowledgment

C.E. acknowledges support from the European Commission through a Marie Curie IOF fellowship (PIOF-GA-2009-252542).

Alben, S., 2008. Optimal flexibility of a flapping appendage in an inviscid fluid. J. Fluid Mech. 614, 355–380.

Blair, G. P., 1996. Design and simulation of two-stoke engines. Society of Automotive Engineers, Inc.

Blom, F. R., Bouwstra, S., Elwenspoek, M., Fluitman, J. H. J., 1992. Dependence of the quality factor of micromachined silicon beam resonators on pressure and geometry. J. Vac. Sci. Techno. B 10 (1), 19–26.

Buchak, P., Eloy, C., Reis, P. M., 2010. The clapping book: Wind-driven oscillations in a stack of elastic sheets. Phys. Rev. Lett. 105 (1), 194301.

Candelier, F., Boyer, F., Leroyer, A., 2011. Three-dimensional extension of Lighthill's large-amplitude elongated-body theory of fish locomotion. J. Fluid Mech. 674, 196–226.

Candelier, F., Porez, M., Boyer, F., 2013. Note on the swimming of an elongated-body in a non-uniform flow. J. Fluid Mech. 716, 616–637.

Dowell, E. H., Hall, K. C., 2001. Modeling of fluid-structure interaction. Annual Review of Fluid Mechanics 33, 445–490.

Eloy, C., Kofman, N., Schouveiler, L., 2012. The origin of hysteresis in the flag instability. J. Fluid Mech. 691, 583–593.

Fletcher, N. N. H., Rossing, T. D., 1998. The physics of musical instruments. Springer.

Ghatkesar, M. K., Braun, T., Barwich, V., Ramseyer, J.-P., Gerber, C., Hegner, M., Lang, H. P., 2008. Resonating modes of vibrating microcantilevers in liquid. Applied Physics Letters 92, 043106.

Heathcote, S., Gursul, I., 2007. Flexible flapping airfoil propulsion at low Reynolds numbers. AIAA J. 45, 1066–1079.

Huang, D. Y., Boyle, K., 2008. Antennas: From Theory to Practice. John Wiley & Sons.

Katz, J., Weihs, D., 1978. Hydrodynamic propulsion by large amplitude oscillation of an airfoil with chordwise flexibility. J. Fluid Mech. 88, 485–497.

Kuperman, V., 2000. Magnetic Resonance Imaging: Physical Principles and Applications. Academic Press.

Lighthill, M. J., 1960. Note on the swimming of slender fish. J. Fluid Mech. 9, 305–317.

Lighthill, M. J., 1971. Large-amplitude elongeted-body theory of fish locomotion. Proc. R. Soc. Lond. B 179, 125–138.

Lopes, J.-L., Païdoussis, M. P., Semler, C., 2002. Linear and nonlinear dynamics of cantilevered cylinders in axial flow. Part 2: the equations of motion. J. Fluids Struct. 16, 715–737.

Marais, C., Thiria, B., Wesfreid, J. E., Godoy-Diana, R., 2012. Stabilizing effect of flexibility in the wake of a flapping foil. Journal of Fluid Mechanics 710, 659.

Michelin, S., Doaré, O., 2013. Energy harvesting efficiency of piezoelectric flags in axial flows. Journal of Fluid Mechanics 714, 489–504.

Michelin, S., Llewellyn Smith, S. G., 2009. Resonance and propulsion performance of a heaving flexible wing. Phys. Fluids 21, 071902.

Païdoussis, M. P., 1998. Fluid-Structure Interactions: Slender Structures And Axial Flow, Volume 1. Academic Press.

Païdoussis, M. P., 2004. Fluid-Structure Interactions: Slender Structures And Axial Flow, Volume 2. Elsevier Academic Press.

Peng, Z., Zhu, Q., 2009. Energy harvesting through flow-induced oscillations of a foil. Physics of Fluids 21, 123602.

Sader, J. E., 1998. Frequency response of cantilever beams immersed in viscous fluids with applications to atomic force microscope. J. Appl. Phys. 84 (1), 64–76.

Singh, K., Michelin, S., de Langre, E., 2012. Energy harvesting from axial fluid-elastic instabilities of a cylinder. Journal of Fluids and Structures 30, 159–172.

Taylor, G. I., 1952. Analysis of the swimming of long and narrow animals. Proceedings of the Royal Society of London. Series A, Mathematical and Physical Sciences 214, 158–183.

Tenney, W. L., 1972. Two-cycle engine resonance exhaust system. U. S. Patent No. 3,665,712.

Turvey, K., 1990. An undergraduate experiment on the vibration of a cantilever and its application to the determination of young's modulus. Am. J. Phys. 58 (5), 483–487.

Wilson, F., Lord Jr., A. E., 1973. Young's modulus determination via simple, inexpensive static and dynamic measurements. Am. J. Phys. 41, 653–656.

Yadykin, Y., Tenetov, V., Levin, D., 2001. The flow-induced vibration of a flexible strip hanging vertically in a parallel flow, part 1: temporal aeroelastic instability. J. Fluids Struct. 15, 1167–1185.

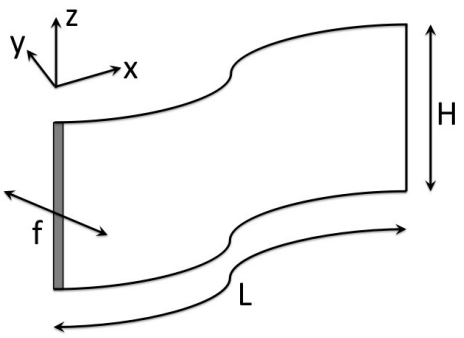

Figure 1: Configuration studied. A flexible plate of length L and width H is clamped in $x = 0$ into a rigid axis that oscillates harmonically in the y-direction with frequency $f = \omega/2\pi$. The trailing edge is free.

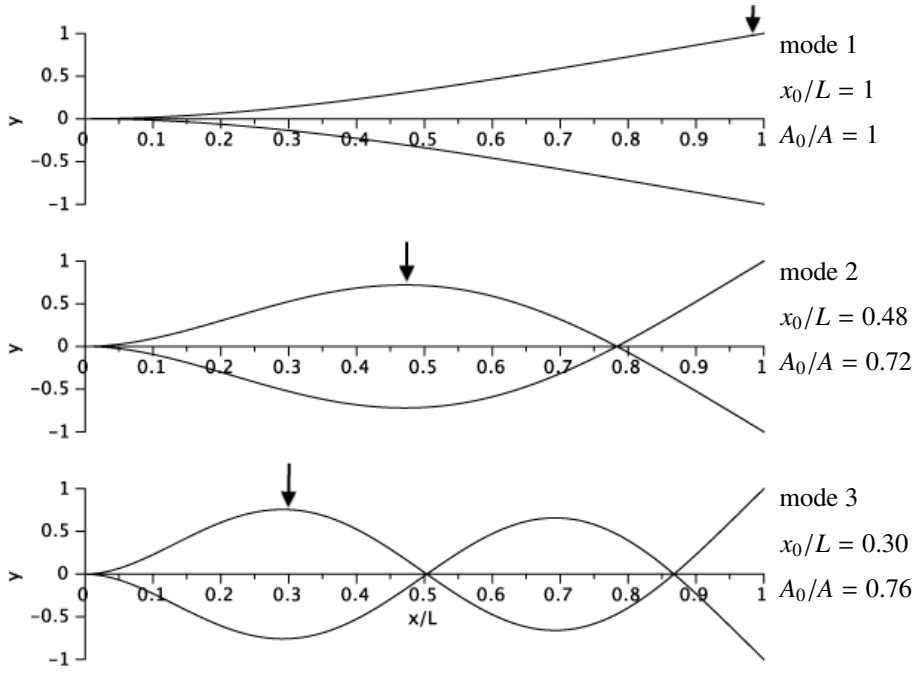

Figure 2: The three first linear eigenmodes with the motion sensor position x_0 marked with an arrow. The amplitude at the sensor position is A_0.

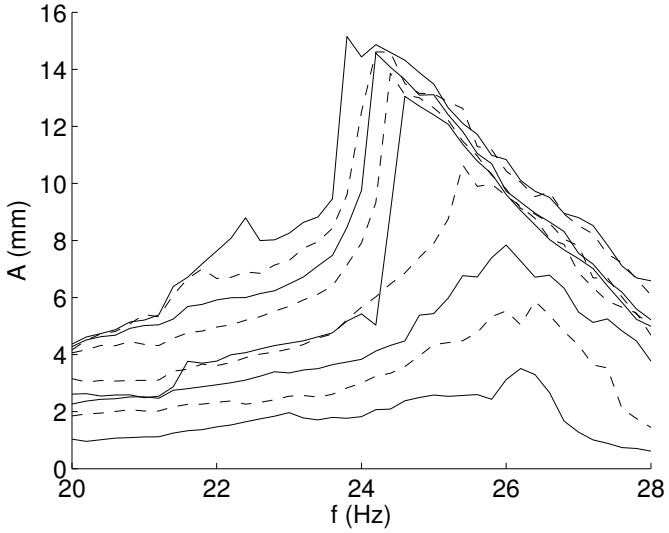

Figure 3: Resonant curves for the third mode of the aluminium plate, for different forcing amplitudes. The larger the forcing amplitude, the higher A.

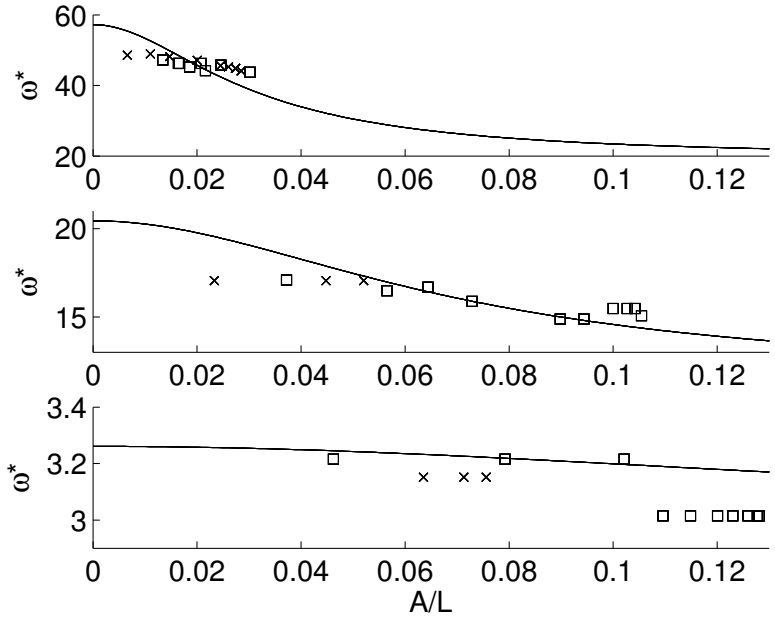

Figure 4: Variation of the resonant frequency with the amplitude for the first three resonant modes (first mode: bottom; second mode: middle; third mode: top). Superimposed plots of the theoretical predictions and the experimental results: plastic plate (□), aluminium plate (×).